JMEPEG (1998) 7:597-600

Penetration in Spot GTA Welds during Centrifugation

D.K. Aidun and S.A. Martin

(Submitted 23 June 1997; in revised form 28 May 1998)

Convective flow during arc welding processes mainly depends on electromagnetic force, Marangoni force, and buoyancy force. The Marangoni flow (caused by surface tension gradient, $d\gamma/dT$) and the buoyancy driven flow are the major factors in controlling weld penetration in austenitic stainless steels, such as types 304 and 316. Alloys 304 and 316 were subjected to a 7 s spot gas-tungsten arc (SGTA) welding at 1 g (g = 9.8 m/s^2) and 5 g accelerations. The welds at 5 g were performed on Clarkson University's multi-gravity research welding system (MGRWS). The cross sections of the fusion zones were polished/etched, and their depth (D) and width (W) were measured to ±0.025 mm. It was determined that the depth/width ratio (D/W) of the welds decreased as the acceleration increased from 1 to 5 g. This result indicates that increase in buoyancy driven flow will produce wider but shallower welds during SGTA welding.

Keywords centrifugation, gas tungsten electrode, Marangoni flow, penetration, welding

1. Introduction

The effects of microgravity (<1 g) on the weld solidification of metals have been investigated to determine the feasibility of the process for space applications. The welding processes that have been studied are electron beam (EB), laser beam (LB), gas-tungsten arc (GTA), plasma arc (PA), gas metal arc (GMA), and brazing (Ref 1).

Electron beam welding has been successfully performed in space by Russian technologists using an electron beam gun developed by the E.O. Paten Electric Welding Institute at Kiev (Ref 2). Laser beam welding on 316 stainless steel in a simulated space environment has been accomplished using the NASA KC-135 laser facility by Wang and Tandon (Ref 3). Using the 70 W laser materials processing system (LAMPS), they determined that wider and deeper welds were obtained in a reduced gravity (0.1 g) environment. Kaukler and Workman (Ref 4) also performed LB welding experiments on the KC-135 laser facility on 304 stainless steel. The greater influence of capillary effects without the influence of gravity was hypothesized to have caused the increased weld penetration, which they observed. Further research work is under way to examine the effect of gravity on the solidification and microstrucure of the laser beam fusion zone (Ref 5, 6).

Computer simulations of plasma arc welding (PAW) in a zero gravity environment have been accomplished by Keanini and Rubinsky (Ref 7). They determined that gravity plays a secondary role in determining the PAW keyhole and weld shape. Domey et al. (Ref 8) performed a computer simulation of the effect of gravity (0.01 to 2 g) on the weld pool size of GTA welds in an alloy similar in properties to 6061 aluminum. They determined that the fusion zone depth/width ratio (D/W) increases with decrease in gravitational acceleration (g = 9.8 m/s^2).

To fully understand the effect of gravity on weld pool geometry and solidification, experiments within a broad spectrum of gravitational accelerations (0.1 to 10 g) should be performed. Therefore, the objective was to experimentally determine the effect of high gravitational acceleration (>>1 g) on the fusion zone shape and size in types 304 and 316 GTA welds.

2. Experimental Procedure

Three heats of 304 and two heats of 316 stainless steels in 50 by 250 mm coupon size (Table 1) were used for this study. Steel wool was used to remove any oxidation from both sides of the coupons prior to spot gas-tungsten arc welding (SGTAW). The tip of the tungsten electrode was also cleaned prior to any welding. The multi-gravity research welding system (MGRWS) (Ref 9), which is a centrifuge with arc welding capabilities, was used to perform 7 s SGTA welds on the stainless steels at 1 and

---

D.K. Aidun and **S.A. Martin,** Mechanical & Aeronautical Engineering Dept., Clarkson University, Potsdam, NY 13699-5725.

Table 1 Composition of the austenitic stainless steels in wt%

	Composition, wt%								
Alloy (thickness)	C	Si	Mn	P	S	Cr	Ni	Mo	Cr_{eq}/Ni_{eq}(a)
304LS (3 mm)	0.1	0.6	1.1	0.03	0.003	18.09	8.45	…	1.76
304HS (3 mm)	0.1	0.4	0.9	0.02	0.008	18.29	8.40	…	1.78
304C (3 mm)	0.1	1.0	2.0	0.05	0.030	18/20	8/12	…	1.53
316LS (2 mm)	0.1	0.5	0.8	0.02	0.001	17.58	11.74	2.07	1.50
316HS (2 mm)	0.1	0.5	0.8	0.03	0.006	17.55	11.83	2.25	1.46

(a) Cr_{eq} = %Cr + %Mo + 1.5x%Si + 0.5x%Nb; Ni_{eq} = %Ni + 30x%C + 0.5x%Mn.

5 g acceleration. Figure 1(a) shows the MGRWS during rotation showing the box on the left that houses the welding torch and the counter balance weight on the right. The power supply and the gas tank are located at the center of the beam. Figure 1(b) shows the inside of the box, and Fig. 1(c) shows the front of the box where a small camera is located for on-line observation of arc welding during the centrifugation process. Because the GTA power supply was not equipped with a high frequency starter, a ≅5 ± 1 mm steel wool ball was placed between the tungsten electrode and the workpiece to initiate the arc. The welding parameters used for this investigation are shown in Table 2. A low speed cut off saw with a 0.375 mm thick diamond blade was used for sectioning the SGTA welds. The position of the weld nugget relative to the diamond blade was measured and controlled using a micrometer. Measurements were made on both sides of the weld nugget, and the position of the cut, P, was determined by $P = -0.375 + (A - B)/2$, where P was the final position of the blade, and A and B were the measurements made at either side of the nugget. The offset of 0.375 mm was to allow for half of the thickness of the blade plus an additional 0.19 mm to account for grinding and polishing. After the welds were sectioned and polished/etched, the fusion zone cross sections were then photographed with a video camera through a tool microscope that was connected to a digital image processing system. The measurements of the depth and width of the fusion zones were recorded in pixels and converted to millimeters. The system allowed the investigator to measure the depth (D) width (W), and the depth/width ratio (D/W) of the fusion zones with an error of ±0.025 mm.

Fig. 1 Multi-gravity research welding system (MGRWS) (a) During rotation. (b) Inside box housing welding torch. (c) Front of box

Table 2 Spot gas tungsten arc (GTA) welding parameters for 1 and 5 g

Property	Value
Current, A	60
Voltage, V	10
Arc time, s	7
Shielding gas	Argon
Gas flow rate, cm^3/min	450
Arc length, cm	0.1
Stick out, cm	0.2
W-2% ThO_2 electrode, cm	0.15
Polarity	DC-EN

1 g corresponds to 0 rpm and 5 g corresponds to 55 rpm. The volume, cm^3, is at STP.

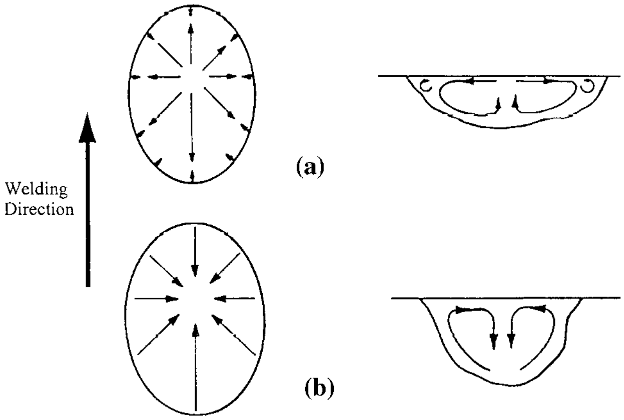

Fig. 2 Fluid flow pattern in molten weld pool with (a) negative surface tension gradient and (b) positive surface tension gradient

3. Results and Discussion

Table 3 shows the effect of gravity on the average size of the fusion zone depth (*D*), the fusion zone width (*W*), and the depth to width ratio (*D*/*W*), respectively. The *D*/*W* decreases as the g level increases for all of the stainless steel SGTA welds. These data show that as buoyancy force increases, the weld zone becomes shallower and the weld bead becomes wider. The reason behind this effect can be one of the following two causes.

It is well known that the three dominant forces controlling convection and flow pattern in an arc welding process at low arc currents are the Marangoni force (MF, or surface tension gradient, $d\gamma/dT$), the electromagnetic force (EMF), and the buoyancy force (BF). The flow pattern of a weld pool due to surface tension gradient is outward if its sign is negative and is inward if its sign is positive, as shown in Fig. 2(a) and 2(b), respectively. The flow pattern of a weld pool due to electromagnetic force is always inward, similar to Fig. 2(b), because the Lorenz force, which must be perpendicular to both the arc current and the magnetic field, must be in radial direction in reference to the weld pool surface. The flow pattern of a weld pool due to buoyancy force is always outward because the fluid at the center of the weld pool is at higher temperature and lower density than the fluid at the edge of the pool. This condition produces an outward flow similar to Fig. 2(a), and it is clear that the outward flow due to buoyancy force increases as the g level increases. Therefore, two cases can exist for this situation:

- Case 1a: inward flow (EMF) + outward flow ($-d\gamma/dT$) + outward flow (BF at 1 g)
- Case 1b: inward flow (EMF) + inward flow ($+d\gamma/dT$) + outward flow (BF at 1 g)
- Case 2a: inward flow (EMF) + outward flow ($-d\gamma/dT$) + 5× outward flow (BF at 5 g)
- Case 2b: inward flow (EMF) + inward flow ($+d\gamma/dT$) + 5× outward flow (BF at 5 g)

For case 1 and 2, as long as the welding parameters are fixed, the EMF effect on the flow pattern and its strength is constant. Comparing case 1a and 2a, the effects of MF and BF on flow pattern are cumulative resulting in shallower but wider fusion zone. For the case of 1b and 2b, although the effects of MF and BF are opposite to each other, in case 2b the effect of BF on the flow pattern is five times greater, which indicates that even if the overall flow is inward, the weld zone still will be wider but shallower. Thus, regardless of either of the cases, the *D*/*W* of the fusion zone will decrease as the g level increases. This is evident from Fig. 3(a) and 3(b) showing the macrograph of SGTA welds done on 316HS at 1 and 5 g, respectively. At 5 g the depth of the fusion zone is smaller and the width is larger as compared to 1 g weld fusion zone resulting in smaller *D*/*W* ratio.

References

1. C. Russel, R. Poorman, C. Jones, A. Nunes, and D. Hoffman, Considerations of Metal Joining Processes for Space Fabrication, *Construction and Repair, 23rd International SAMPE Technical Conference,* SAMPE, 21-24 Oct 1991, p 555-556
2. B. Irving, Electron Beam Welding, Soviet Style: A Front Runner for Space, *Weld. J.,* July 1991, p 55-59

Table 3 Average depth, width, and depth/width ratio of GTA fusion zone

	Average depth, mm		Average width, mm		Average depth/width	
Alloy	**1 g**	**5 g**	**1 g**	**5 g**	**1 g**	**5 g**
304LS	1.09 ± 0.17(a)(b)	0.97 ± 0.1(b)	3.48 ± 0.02	3.51 ± 0.05	0.31 ± 0.15	0.27 ± 0.1
304HS	1.33 ± 0.01(c)	1.11 ± 0.3(b)	3.39 ± 0.01	3.43 ± 0.01	0.39 ± 0.01	0.32 ± 0.3
304C	1.1 ± 0.01(c)	0.91 ± 0.05(c)	3.7 ± 0.03	3.66 ± 0.01	0.29 ± 0.02	0.25 ± 0.05
316LS	1.25 ± 0.02(c)	1.3 ± 0.13(b)	4.02 ± 0.01	4.36 ± 0.01	0.31 ± 0.01	0.29 ± 0.13
316HS	1.26 ± 0.01(c)	0.79 ± 0.11(c)	3.41 ± 0.05	3.59 ± 0.01	0.37 ± 0.04	0.22 ± 0.11

(a) Coefficient of variation. (b) 3 welds. (c) 2 welds

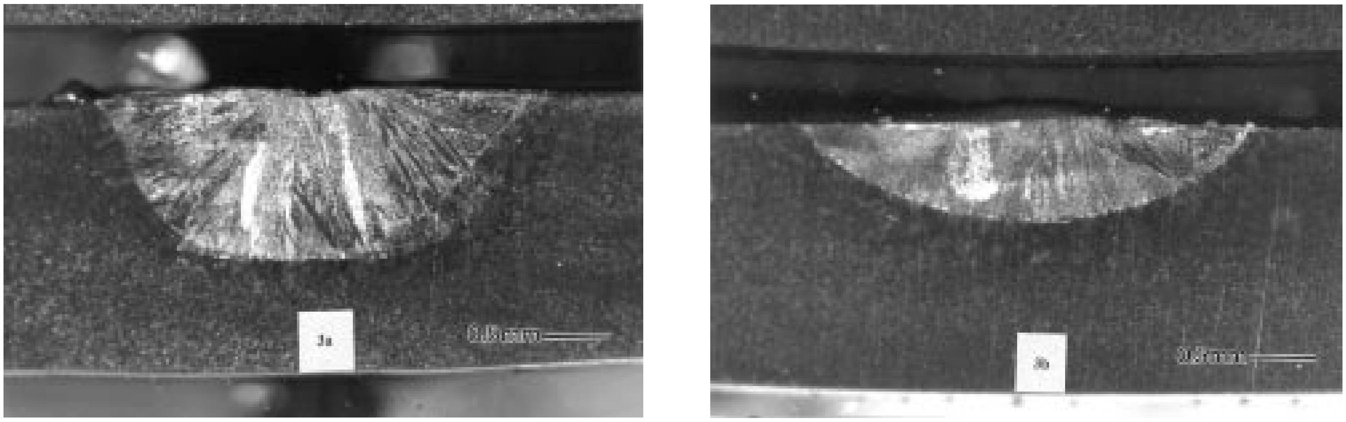

Fig. 3 7 s GTA spot weld performed on 316HS. (a) 1 g. (b) 5 g

3. G. Wang and K.N. Tandon, the Microstructural Changes during Welding of Stainless Steel under Reduced Gravity Environment, *Microgravity Sci. Technol.,* V1/2, 1993, p 96-100
4. W.F. Kaukler and G.L. Workman, Laser Welding in Space, *Proc. from the Conf. Welding in Space and the Construction of Space Vehicles by Welding,* NASA/Microgravity Materials Processing in Space, 24-26 Sept 1991, p 318-334
5. L.A. Boatner, S.A. David, and G.L. Workman, Gravitational Effects on the Development of Weld-Pool and Solidification Microstructures," presented at the Microgravity Materials Science Conference (Huntsville, AL), NASA/Microgravity Materials Processing in Space, May 1994
6. J. Singh, "Gravitational Effect on the Development of Laser Weld-Pool & Solidification Microstructure," presented at the Microgravity Materials Science Conference, (Huntsville, AL), NASA/Microgravity Materials Processing in Space, June 1996
7. R.G. Keanini and B. Rubinisky, Plasma Arc Welding under Normal and Zero Gravity, *Weld. J.* June 1990, p 41-49
8. J. Domey, D.K. Aidun, G. Ahmadi, L.L. Regel, and W.R. Wilcox, Numerical Simulation of the Effect of Gravity on Weld Pool Shape, *Weld. J.,* Aug 1995
9. Centrifuge Designed for Welding and Casting in High Gs, "News of the Industry," *Weld. J.,* June 1997, p 8